International Journal of Earth & Environmental Sciences
Vol. 11, No. 1, 2026, pp. 134-157

http://ijees.ielas.org
ISSN: 2545-4161

HYDROGEOCHEMICAL CHARACTERIZATION ASSESSMENT OF GROUNDWATER WITHIN IMICHAEL OKPARA UNIVERSITY OF AGRICULTURE AND ENVIRONS, UMUDIKE SOUTHEASTERN NIGERIA

***[1]Iyi, Emmanuel Chibuike and *[2]Okoro, Joel Ejiofor**

*1Enugu State University of Science and Technology (ESUT), Enugu State, Nigeria

*2Geology Department, Michael Okpara University of Agriculture, Umudike, P.M.B. 7267, Umuahia, Abia State, Nigeria.

*Corresponding author: innocentezeugwu38@gmail.com

Received: 2026-06-02 Accepted: 2026-09-11 Published online: 2026-09-13

Abstract

Groundwater serves as the primary source of potable water for Michael Okpara University of Agriculture, Umudike, and its surrounding agrarian communities in southeastern Nigeria. As population growth and more intensive farming increases, the demands for regular monitoring of groundwater quality are required to maintain long-term viability and protect health. Here, the hydrogeochemical properties, spatial patterns, and suitability of groundwater for both consumption and irrigation across the area are assessed. In total, eleven boreholes were methodically sampled and tested for key physicochemical indicators (pH, conductivity, and dissolved-solids content), major dissolved ions…, and trace elements (Cu, Mn, Cr, Cd, Pb, Zn, Fe, As, Mo, and V). Standard methods were applied for hydrochemical interpretation, such as Piper plotting, Gibbs plotting, and computation of the Sodium Adsorption Ratio (SAR); and contour maps were used to examine spatial differences. The findings show Ca–Mg–HCO_3 water types prevail, implying that interaction between water and the Benin Formation strongly shapes the chemistry. For major cations, the ranking is Ca > Mg > Na > K. Bicarbonate is the principal anion. Evaluation of the Gibbs plots points to rock breakdown by weathering as the key process controlling groundwater composition. In general, measured heavy metals are small in amount and lie within limits accepted by the WHO. Potentially harmful constituents, including Cd and Pb, were mostly not-detected, and only a few outliers hint at site-specific human-related contributions. Correlation testing indicates pronounced positive links for Fe with Cr ($r = 0.958$) and for Fe with Mn ($r = 0.690$), reinforcing mineral alteration as the dominant origin. Spatial plotting highlights clear spatial trends, with concentrated zones of Cr and As in the west-central area and a northwest-to-southeast decline for Zn. Even with these irregularities, the groundwater resource is, overall, largely free from contamination. Small SAR values demonstrate very good irrigation suitability and indicate no sodium-related risk. It is inferred that groundwater in the area shows chemical steadiness and is appropriate for household needs as well as farming. The results is an essential reference point for sustainable groundwater oversight and environmental surveillance within the region.

Keywords: Groundwater quality; Hydrogeochemistry; Heavy metals; Water–rock interaction; Sodium Adsorption Ratio (SAR).

INTRODUCTION

As a vital freshwater reserve, groundwater supports drinking needs, farming, and industrial use, especially where rivers and lakes are limited or unreliable (United Nations Educational, Scientific and Cultural Organization, 2022; World Health Organization, 2017). Across numerous Nigerian communities, it provides the main supply of safe-to-drink water because it is fairly easy to obtain and is commonly regarded as clean (Adelana and MacDonald, 2008). Even so, groundwater quality is not automatically assured, since it depends heavily on the rock units it passes through and on human actions like agricultural methods, dumping of wastes, and construction activities (Appelo and Postma, 2005; Li et al., 2019). Therefore, carrying out regular checks of groundwater quality via geochemical assessment is necessary to protect both its safety and long-term use (Subramani et al., 2010; Egbueri and Unigwe, 2020).

At Michael Okpara University of Agriculture, Umudike, located in Abia State, daily water demand for students, employees, host communities, cattle and other domestic animal populations is met mainly through groundwater sources, including boreholes. As the university area and its surroundings experience rising population and more intensive farming, worries are increasing about possible pollution of the groundwater system (Egbueri, 2020; Ukah et al., 2019). Through fertilizer inputs, pesticide application, and poor handling of wastes, undesirable materials may enter underground zones and, in turn, modify the natural chemistry of the groundwater (Zhang et al., 2018; Pallavi et al., 2023).

A geochemical appraisal of groundwater entails organized testing of physical and chemical indicators, such as pH, conductivity, total dissolved solids, and levels of key ions, including calcium, magnesium, sodium, potassium, chloride, sulfate, and bicarbonate (World Health Organization, 2017). Beyond these, investigations also cover trace constituents and suspected pollutants so their amounts and possible health effects can be assessed (Li et al., 2019; Egbueri and Unigwe, 2020). With these results, it becomes possible to recognize the leading processes influencing groundwater composition in the area, such as dissolution of minerals, ion exchange reactions, and human-driven impacts (Appelo and Postma, 2005; Subramani et al., 2010).

The purpose of this research is to evaluate groundwater geochemistry within Michael Okpara University of Agriculture, Umudike, so that its fitness for drinking and for irrigation can be determined. Using established guidelines—such as those issued by the World Health Organization—the measured values will be checked against accepted limits to see if the groundwater falls within allowable quality ranges (WHO, 2017). Results from the work will supply useful input for managing water resources and will aid in forming measures intended to protect groundwater quality. In the end, maintaining access to clean, safe groundwater remains essential for public health protection and for sustainable progress within the university area and nearby locations (UNESCO, 2022).

DESCRIPTION OF THE STUDY AREA

Location and Geology

Umudike, in Ikwuano Local Government Area of Abia State in southeastern Nigeria, is the location of the study (Fig. 1). From Umuahia, the state capital, the site is roughly 9–10 km to the east. The university situated along the Umuahia–Ikot Ekpene federal road, an important corridor connecting multiple states in the southeast and south-south. In spatial terms, the area falls between 5°28′N and 5°30′N latitude, and between 7°31′E and 7°33′E longitude. As reported by Igboekwe and Akankpo (2012), heights across the study zone vary approximately from 60 to 180 m above sea level. It lies in a humid rainforest belt characterized by heavy rainfall and active agriculture (Chukwunenyoke, 2019). Most neighboring settlements depend on farming, aligning with the institution's agricultural mandate (Chukwunenyoke, 2019).

As indicated in Figure 2, the local geology shows that the area lies within the eastern Niger Delta sedimentary basin. In broad terms, delta-related marine deposits dating from the Cretaceous through the Recent underlie the region (Igboekwe et al., 2012). The setting is part of the Niger Delta's Benin Formation, also known as the Coastal Plain Sands (Igboekwe and Akankpo, 2012; Chukwunenyoke, 2019). Within the locality, two main units are present: Benin Formation (Coastal Plain Sands), made up largely of unconsolidated coarse-to-medium sand and noted for very high permeability. In this area, it constitutes the principal aquifer framework. The second geologic unit present, the Bende–Ameki Formation, consists of sandstone beds (commonly coarse), along with clay and shale horizons, plus siltstone and occasional limestone. The Bende-Ameki Formation shows lateral variation in lithology within the study area (Igboekwe and Akankpo, 2012). From a hydrogeologic perspective, the dominance of sandy units makes groundwater resources abundant. Aquifer bodies are typically unconfined to partly confined, occurring within sandy strata (Igboekwe et al., 2012). Nonetheless, the groundwater can be mildly acidic, so treatment may be needed before it is suitable for drinking (Igboekwe et al., 2012).

Obi and Udo (2011) stated that soils in the area are mainly sandy to loamy, having formed from coastal plain sand materials. Because rainfall is intense, the soils are also very prone to erosion. While the soils can support farming, they still demand appropriate management practices.

MATERIALS AND METHODS

Sample Collection and Preservation

Water samples from boreholes were taken at chosen locations throughout the study area, as presented in table 1. Using a random selection method, twelve (12) representative sampling sites were chosen. Sample collection was done with clean 1.5 L

polyethylene containers. Before use, the containers were conditioned with 10% nitric acid (HNO_3) and then washed with distilled water. To obtain a representative sample, each borehole was pumped for 5–10 minutes prior to filling the bottles. For cation and heavy-metal testing, samples were preserved by adding HNO_3 until pH was below 2. Every sample was labeled correctly and kept in an ice chest at about 4°C until laboratory work commenced. By using these steps, sample quality was maintained and risks of contamination or chemical change were minimized.

In-situ Measurement of Physicochemical Parameters

At each site, portable instruments were used to take field readings for pH and electrical conductivity (EC). Measurements were made right after collection so that exposure-related changes would not occur.

The laboratory results were converted and handled in meq/L, after which SAR, Gibbs, and Piper plots were produced and interpreted.

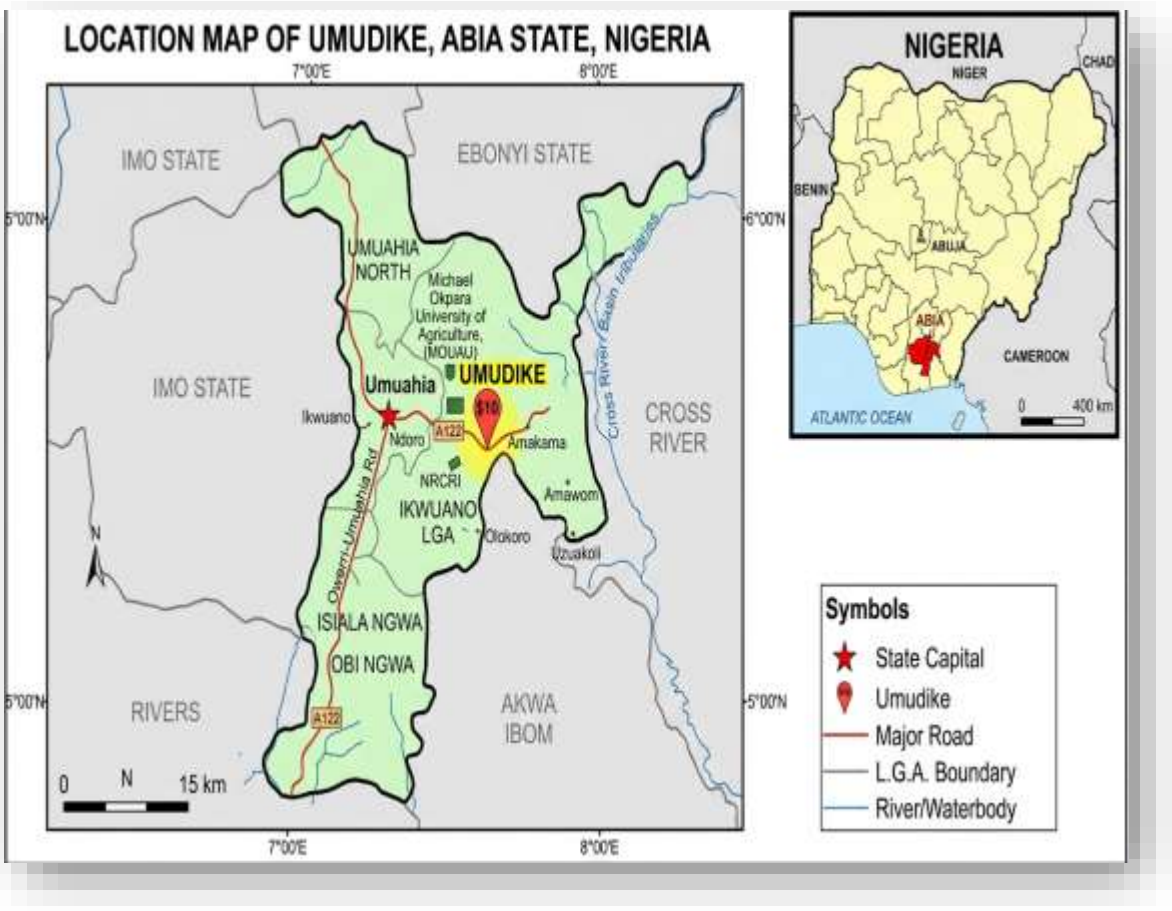

Figure 1: *Location map of the study area (Insert is map of Nigeria).*

International Journal of Earth & Environmental Sciences
Vol. 11, No. 1, 2026, pp. 134-157
http://ijees.ielas.org
ISSN: 2545-4161

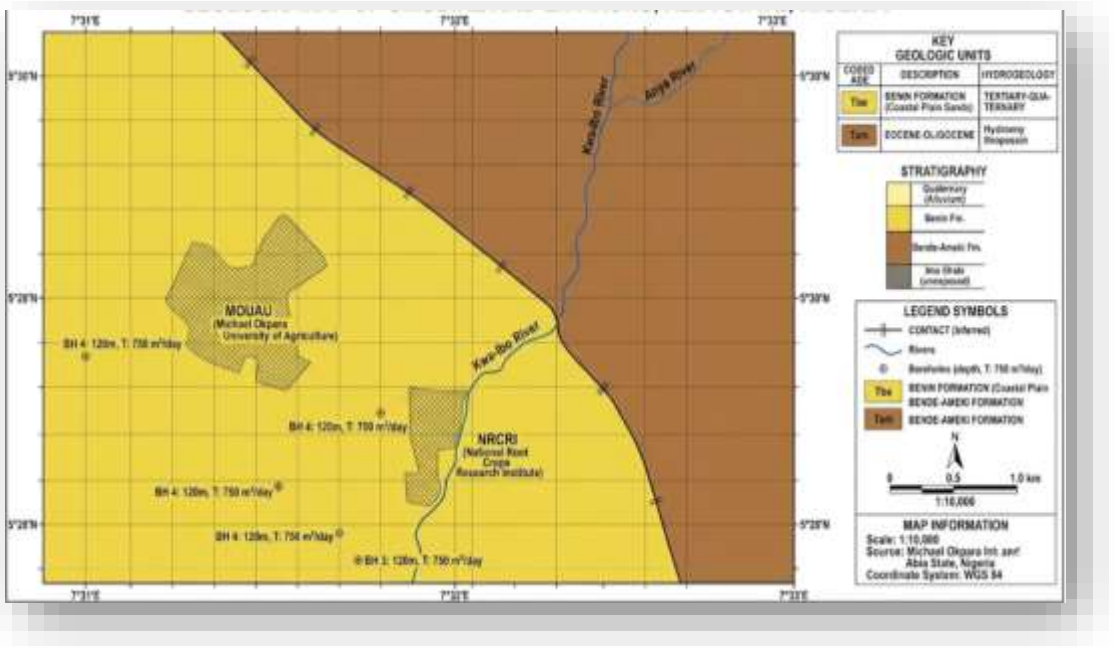

Figure 2: *Geological map of Umudike showing the study area (Adopted from Amos-Uhegbu et al., 2017).*

Table 1
Sample collection points and their Coordinates

Location	GPS Coordinates
Admin	5º 28'44'' N 7º 32' 41''E
Chapel of Revelation	5º 28' 30''N 7º 32' 37''E
NDDC Hostel	5º 28' 36''N 7º 32' 28''E
CEET	5º 28' 47''N 7º 32' 46''E
CBN Building	5º 28' 38''N 7º 32' 18''E
IBB Hostel	5º 28' 52''N 7º 32' 30''E
COLNAS	5º 28' 37''N 7º 32' 37''E
CCSS	5º 28' 90''N 7º 32' 38''E
Library	5º 28' 66''N 7º 32' 59''E
Female Hostel	5º 28' 55''N 7º 32' 32''E
3-Winged Hall	5º 28' 41''N 7º 31' 58''E
GEJ Hostel	5º 28' 40''N 7º 31' 57''E

RESULTS AND DISCUSSION

Physicochemical Categorization of Groundwater

As presented in Table 2, groundwater chemistry in the investigated area is mainly controlled by the amounts of the principal cations (Ca2+, Mg2+, Na+, K+) and the main anions (Cl−, SO42−, HCO3−, CO32−), and these ions signal how subsurface water interacts with the surrounding rock. Data produced from twelve sampled points indicate waters largely governed by alkaline-earth elements together with weak-acid anions, implying a recognizable geochemical signature consistent with the Benin Formation.

Composition and Distribution of Cations

Among the major cations, the arrangement remains uniform, progressing as Ca>Mg>Na>K. *Calcium (Ca2+) and Magnesium (Mg2+):* In this set, calcium ranks first, measuring 52.1 mg/L at COLNAS and rising to 112.22 mg/L at the CBN Building. Magnesium values are comparable in pattern, extending from 31.62 mg/L up to 68.1 mg/L. Elevated levels of these alkaline-earth constituents, notably around sites such as the IBB and Female Hostels, point to substantial dissolution of carbonate-rich minerals within the sedimentary sequence.

Sodium (Na+) and Potassium (K+): By contrast, alkali elements occur at comparatively small amounts. Sodium varies between 0.6 mg/L and 2.59 mg/L, whereas Potassium stays very low and shows little variation, with a mean near 0.33 mg/L. Such subdued concentrations imply limited contribution from silicate breakdown or human-related sources like household effluent.

Characteristics and Hydrochemical Facies of Anions

Bicarbonate (HCO_3^{-}) and Chloride (Cl^-) constitute the main anions, whereas sulfate (SO_4^{2-}) and Carbonate (CO_3^{2-}) appear only at trace levels.

Bicarbonate (HCO_3^-): Across every station, bicarbonate remains consistently elevated, lying between 50.56 mg/L and 59.75 mg/L. The prominence of HCO_3^- aligns with recharge-area groundwater in the Niger Delta, where rainfall enriched in CO_2 reacts with minerals in soils and the vadose zone.

Chloride (Cl−): Chloride shows clear spatial differences, with the highest value at 66.45 mg/L (Chapel of Revelation) and the lowest at 21.33 mg/L (GEJ Hostel). Although all measurements remain within drinking-water limits, the changes likely relate to small-scale differences in soil transmissivity or inputs from atmospheric fallout.

Minor Anions: Sulfate is essentially absent, with all values below 0.1 mg/L, pointing to minimal dissolution of sulfur-containing minerals and possibly reducing settings that limit sulfate persistence.

Geochemical Implications

Collectively, the ion relationships indicate a Ca-Mg-HCO3 water class, a conclusion reinforced by Gibbs-plot reading that identifies rock control as the dominant process. When calcium and bicarbonate are comparatively high while heavy metals remain at trace levels, it suggests an unpolluted groundwater system in which natural rock–water reactions—especially weathering of carbonate and ferromagnesian phases—supply most dissolved material. Accordingly, the findings indicate that the groundwater is chemically stable and can serve domestic and farming needs without major pretreatment for the principal ions.

Table 2
Physiochemical parameters and major ionic concentrations in the study area

Location	*pH*	*EC (us)*	*K (mg/l)*	*Ca (mg/l)*	*Na (mg/l)*	*Mg (mg/l)*	*PO4 (mg/l)*	*SO4 (mg/l)*	*Cl (mg/l)*	*NO2 (mg/l)*	*HCO3 (mg/l)*	*CO_3^{2-} (mg/l)*
Admin	6.6	12.65	0.316	96.19	2.57	58.37	-ve	0.016	65.48	-ve	50.56	0.56
Chapel of Revelation	6.2	12.71	0.312	96.21	2.51	58.36	-ve	0.016	66.45	-ve	59.62	0.63
NDDC hostel	6.5	16.46	0.306	88.18	1.64	55.17	0.04	0.024	52.44	0.059	59.75	0.59
CEET	6.4	16.64	0.308	60.18	1.63	36.48	0.25	0.031	41.34	0.02	55.69	0.58
CBN Building	6.2	15.42	0.343	112.22	0.6	68.09	0.26	0.041	24.14	-ve	54.48	0.58
IBB hostel	5.8	12.23	0.341	112.18	0.68	68.1	0.07	0.055	41.34	0.002	56.84	0.68
COLNAS	4.9	15.53	0.288	52.1	1.46	37.62	0.02	0.031	37.96	0.009	51.23	0.52
CCSS	6.4	13.87	0.292	52.12	1.49	31.62	-ve	0.046	43.23	-ve	58.77	0.772
Library	5	13.36	0.343	88.41	2.59	57.38	0.02	0.044	24.12	-ve	59.43	0.78
Female Hostel	5.7	12.7	0.341	112.18	0.6	68.09	-ve	0.035	24.12	-ve	58.96	0.64
3-Winged Hall	6.6	22.74	0.363	60.12	1.63	54.5	0.21	0.016	22.14	-ve	56.52	0.63
GEJ hostel	6.5	28.45	0.354	78.65	1.62	36.52	0.22	0.084	21.33	-ve	54..11	0.56

Heavy Metal Concentrations in Groundwater

Across the area (Table 3), analyzed groundwater for selected metals (Cu, Mn, Cr, Zn, Fe, As, Mo, Cd, Pb and V) generally yields low to trace amounts. Relative to World Health Organization standards, the majority of results remain within allowable drinking-water thresholds as discussed below.

Copper (Cu)

Measured Copper ranges from undetected to 0.002 mg/L, and the mean±sd is reported as 0.00667±0.0036 mg/L. Such small concentrations point to little human-derived contribution and no clear evidence of major industrial pollution.

In addition, the measurements are far below the WHO (2017) reference level of 2.0 mg/L, implying no associated health concern.

Manganese (Mn)

Manganese is similarly low, from 'not detected' to 0.02 mg/L. The mean±sd is given as 0.026±0.0163 mg/L. These results comply with the WHO (2017) acceptable limit of 0.4 mg/L.

The low Mn observed is most reasonably linked to natural geological inputs, especially alteration of ferromagnesian minerals.

Chromium (Cr)

For Chromium, results range from non-detectable to 0.002 mg/L, with an average of 0.034±0.0397 mg/L. These levels are minimal and suggest that contamination is insignificant.

Zinc (Zn)

Zinc is also extremely small (~0.001 mg/L), ranging from non-detectable to 0.001 mg/L, with a mean±sd of 0.0031±0.00145 mg/L. Relative to the 3.0 mg/L allowable level (WHO…), the values are far lower. The Zn results therefore indicate very limited contamination across the area.

Although Zn can move readily in groundwater, its scarcity here implies only minor influence from human activities.

Cd and Pb

Cadmium (Cd) and lead (Pb) are mostly below detection throughout the area, indicating that both are essentially absent or occur only at very low background amounts. The recurring "-ve" entries for the two variables point to little widespread input and indicate generally favorable groundwater quality regarding these hazardous elements. For lead (Pb), one clear exception occurs, where 0.025 is measured at a single sampling point. Because other samples are largely non-detect, this lone value points to a local Pb source rather than a broad regional control. A localized rise like this may stem from point contributions, including human actions such as dumping, industrial remnants, or the breakdown of materials containing lead. Since nearby samples lack Pb, its occurrence appears tightly confined and not governed by regional geochemical controls.

Cadmium (Cd), however, appears slightly more often than Pb, though still infrequently overall. Two sites show detectable values of 0.003 and 0.001, while the remaining samples stay below detection. These small detections imply minor, localized inputs, potentially tied to farming practices such as phosphate fertilizer application or other dispersed human sources. That Cd and Pb do not coincide further supports the view that they arise from separate sources or follow different geochemical controls. In summary,

both Cd and Pb show isolated departures within a setting that is otherwise environmentally clean.

Iron (Fe)

Iron ranges from non-detected to 0.003 mg/L, and the mean±sd is stated as 0.0219±0.027 mg/L, which remains within allowable limits. The measured amounts are below the WHO (2017) aesthetic threshold of 0.3 mg/L.

Overall, the outcome indicates only limited iron release even if reducing conditions exist. In addition, the small Fe detected could reflect weathering of iron-rich minerals or mildly acidic groundwater conditions noted in the physicochemical findings.

Arsenic (As)

Most samples showed arsenic at levels under the detection threshold (-ve). Measured values span from 'not detected' up to 0.046 mg/L, and the mean is 0.046±0.00. These findings imply no toxic pollution and indicate no effect from industrial effluent or arsenic-bearing rock units.

Molybdenum (Mo)

Molybdenum values are similarly low. The measured interval extends from non-detects to 0.002 mg/L, while the reported mean is 4.365±12.956 mg/L. In general, groundwater Mo in the investigated area remains within permissible levels and is probably sourced from minor dissolution of trace minerals.

Vanadium (V)

Vanadium was absent in most readings (-ve). This points to an insignificant contribution from either natural geology or human activities.

Correlation Analysis of Heavy Metals

As presented in Table 4, the correlation results show clear geochemical links among the evaluated heavy metals, reflecting influences from both natural factors and human activity on groundwater chemistry. The exceptionally high positive link between Cr and Fe (r = 0.958) points to a shared geologic source, most probably tied to the breakdown and dissolution of iron-bearing minerals that also contain chromium. Similarly, the strong relationship between Mn and Fe (r = 0.690) reinforces this view, since both commonly occur together in ferromagnesian minerals and tend to be released under comparable redox settings. Collectively, these patterns indicate that lithology and water–rock interactions are key controls on how these elements are distributed.

By comparison, the pronounced positive relationship between Cu and Cd (r = 0.738) suggests another governing process, potentially associated with human-derived inputs. Such paired behavior is frequently connected with farming practices, refuse disposal, or other anthropogenic sources where both metals enter the environment together. In addition, the mid-level correlation between Mn and Cr (r = 0.595) implies some shared behavior, perhaps indicating partial convergence between primary mineral sources and secondary processes such as adsorption or co-precipitation.

Table 3
Heavy Metal distributions across the study area

Location Name	GPS Coordinates (N, E)	Elevation (ft)	Cu	Mn	Cr	Cd	Pb	Zn	Fe	As	Mo	V
Admin	5°28′44″N, 7°32′41″E	136	0.005	0.025	-ve	-ve	-ve	0.001	0.023	-ve	0.010	-ve
Chapel of Revelation	5°28′30″N, 7°32′37″E	399	0.004	0.022	-ve	-ve	-ve	0.004	0.019	-ve	0.008	-ve
NDDC Hostel	5°28′36″N, 7°32′28″E	378	-ve	0.054	0.090	-ve	-ve	-ve	0.096	-ve	0.162	-ve
CEET	5°28′47″N, 7°32′46″E	1047	0.002	0.011	-ve	-ve	-ve	0.006	-ve	-ve	0.162	-ve
CBN Building	5°28′38″N, 7°32′18″E	376	0.006	0.013	-ve	-ve	-ve	0.004	-ve	-ve	0.025	-ve
IBB Hostel	5°28′52″N, 7°32′30″E	378	-ve	0.008	-ve	-ve	-ve	0.002	0.006	-ve	0.002	-ve
COLNAS	5°28′37″N, 7°32′37″E	362	-ve	0.006	-ve	-ve	-ve	0.003	0.007	-ve	0.014	-ve
CCSS	5°28′30″N*, 7°32′38″E	398	-ve	-ve	-ve	-ve	0.025	-ve	-ve	0.046	43.230	-ve
Library	5°28′56″N*, 7°32′59″E	432	-ve	-ve	-ve	-ve	-ve	0.003	0.003	-ve	0.016	-ve
Female Hostel	5°28′55″N, 7°32′32″E	219	-ve	0.042	-ve	-ve	-ve	0.002	0.008	-ve	0.018	-ve
3-Winged Hall	5°28′41″N, 7°31′58″E	261	0.011	0.044	0.010	0.003	-ve	-ve	0.017	-ve	-ve	-ve
GEJ Hostel	5°28′40″N, 7°31′57″E	408	0.012	0.038	0.002	0.001	-ve	-ve	0.018	-ve	-ve	-ve

Table 4
Correlation analysis of heavy metals in the study area

	Cu	Mn	Cr	Cd	Pb	Zn	Fe	As	Mo	V
Cu	1	0.419	-0.165	0.738	-0.239	-0.276	-0.049	-0.239	-0.24	—
Mn		1	0.595	0.454	-0.372	-0.493	0.69	-0.372	-0.371	—
Cr			1	-0.008	-0.104	-0.379	0.958	-0.104	-0.101	—
Cd				1	-0.118	-0.432	0.013	-0.118	-0.12	—
Pb					1	-0.332	-0.196	1	1	—
Zn						1	-0.442	-0.332	-0.331	—
Fe							1	-0.196	-0.194	—
As								1	1	—
Mo									1	—
V										

SPATIAL VARIATION OF HEAVY METALS

Cu: As shown in Figure 3, contour display indicates notable spatial non-uniformity in Cu across the area, combining localized highs with broader gradients.

To begin with, the maximum Cu values appear in the southwest of the study area (lower left), reaching about 0.0095 mg/L (red–orange region). Moving away from that zone, Cu concentrations steadily drop toward the central and northern sections, showing a strong southwest-to-northeast gradient from higher to lower levels. This arrangement implies a likely source or control situated in the southwestern sector—such as rock type, human influence, or geochemical buildup.

Another key aspect is a small, localized elevated feature in the northwest-central sector, shown as a compact circular green area bounded by closely spaced contours (~0.002 mg/L). The dense contour pattern indicates a sharp change in concentration, suggesting a point influence or localized geochemical control (e.g., a mineralized patch, a dumping location, or recharge-related effects).

Conversely, the central and northeastern parts of the map are characterized by low Cu levels (blue to purple shades, around 0.002 mg/L or less). In these zones, contours are more spread out, indicating a mild gradient and fairly consistent low values. This points to possible dilution, weaker mineralization, or less anthropogenic effect.

Overall, these spatial features indicate that Cu distribution is shaped by both regional drivers (e.g., geological setting, groundwater movement) and local factors (e.g., contamination hotspots or mineralization areas) within the study area.

Mn: The Mn contour map (Fig. 4) presents a clear spatial configuration marked by a centrally elevated zone with concentrations diminishing outward.

Peak Mn occurs in the central-west part of the study area, where levels rise to roughly 0.06 mg/L (red area). Around this core, nested contour rings (0.055, 0.05, 0.045 mg/L) show a progressive decrease with distance from the enrichment center. The somewhat tight contour spacing near this feature indicates a moderately sharp gradient, consistent with a localized source or an accumulation process.

Moderate Mn values occur in the south and southeast (roughly 0.035–0.04 mg/L), depicted in green tones. Here, the broader and smoother contour spacing suggests a more gradual reduction in concentrations.

Low Mn dominates the north and northeast (≤0.02 mg/L), illustrated by blue-to-purple colors. Widely spaced contours in this sector indicate consistently low Mn and limited spatial change.

A small low-value pocket (dark blue) is also visible in the southwest, indicating localized reduction or dilution, potentially linked to hydrogeologic factors such as recharge effects or contrasting lithology.

In summary, Mn varies spatially with a high zone near ~0.06 mg/L consistent with possible point input or geogenic enrichment, followed by a systematic outward decline that produces a radial pattern. Toward the northern and northeastern sectors, concentrations are lower and more uniform.

This distribution indicates Mn is governed by both local geochemical influences (e.g., dissolution of minerals or anthropogenic contributions) and broader controls such as groundwater transport and dilution.

Cr: In Figure 5, the contour map for Chromium (Cr) shows a tightly confined pattern, standing in sharp contrast to the earlier map's wide-area gradient.

Its' most notable characteristic is a strong, isolated anomaly positioned near the center-left margin.

At the core, the red-to-orange target-like zone contains the highest readings, and the labeled contours show amounts above 0.05. A compact, rounded signature like this usually points to a single source or a narrowly focused geological/environmental driver, not a large-scale regional process.

Around that central high, the change in values is exceptionally abrupt. Over a small distance, the colors shift quickly from orange near 0.05 to deep blue around 0.005.

The fastest decline occurs toward both the north and the south, whereas a somewhat gentler extension or spread trends eastward.

Across most of the site (including all of the right-hand half and the northeastern quarter), Cr remains very low. This appears as pale violet and light blue tones, with values trending to zero or even marginally negative (as suggested by the -0.005 artifact at the upper-left).

A small, broad rise is also present in the southwest corner, where levels increase modestly to about 0.01. Compared with the main hotspot this is far weaker, but it still signals a local difference relative to the largely empty northeast.

To conclude, Cr varies little across most locations, interrupted mainly by one intense peak centered in the west-central zone.

Cd: The Cd contour map in Figure 6 shows a strong large-scale slope, with the greatest amounts in the southwest and a steady reduction toward the north and northeast. Near (5.478, 7.533)—the 3-Winged Hall—a clear hotspot appears, and Cd attains about 0.003, shown by a bright red area on the contours. By comparison, the northern part—especially above latitude 7.542—shows very small to nearly zero values, reflected by widespread purple coloring.

Examining the contours indicates that Cd spread differs notably across the map. In the southwest, the contours are packed close together, signaling a sharp drop from the hotspot to lower values over a short span. In the east and southeast, however, the spacing opens up and the decline becomes gentler, with concentrations tapering more slowly across a broader zone. This implies wider, less sudden dispersion in that direction than the steep decrease seen toward the north.

Taken together, the map indicates one Cd point origin in the southwestern quadrant. From there, levels expand outward, creating a strong central core and a weaker, more diffuse reach toward the southeast. Even with this localized increase, most of the area stays at background or near-zero Cd, implying that broad contamination is limited.

Pb: Figure 7 shows that Lead (Pb) follows a clear, steady rise from west toward east. The left half contains very low amounts that largely match background, while values

increase progressively moving to the right. The greatest levels occur along the eastern edge, most notably around the mid-right area, where the peak is roughly 0.019 and is depicted by strong red coloration.

Rather than forming a single tight hotspot like some other elements, Pb forms a wide, continuous zone of buildup instead of one concentrated point. The west remains dominated by near-zero readings, with only small increases seen moving east across broadly spaced contours in the northwest. This points to a gradual emergence of Pb from the west that shifts into much higher levels toward the east.

Assessing the gradient shows the sharpest rise in the middle portion, where tight contour spacing marks a steep jump from moderate to high values. The contour bands run mainly vertical, indicating that variation is driven chiefly by an east–west pattern with little north–south effect. In sum, the layout implies a strong environmental or geological influence pushing Pb accumulation toward the eastern section, while the west stays comparatively clean.

Zn: Zinc (Zn) displays a distinct diagonal decline from northwest toward southeast across the site (Fig. 8). The maximum values lie in the northwest corner, reaching about 0.0055 and shown by vivid orange-red tones. The southeast quarter, in contrast, is the minimum zone, with values nearing zero and colored light purple. In general, Zn decreases steadily from the upper-left toward the lower-right.

The left side of the map shows considerable complexity and small-scale variability. Beyond the main high in the northwest, another raised area appears in the lower-left to western portion, where values reach around 0.003. Near that elevated patch, a clear localized low occurs, where Zn falls quickly to roughly 0.0015 even though higher values surround it. These shifts, together with tightly packed contours, indicate strong spatial variation and suggest more than one controlling influence in the western area.

Gradient evaluation also shows the most abrupt drop close to the northwest, where values fall rapidly across a short distance. Farther east, the contours become more evenly spaced and broader, indicating a slower, steadier move down toward background levels. Overall, the distribution points to a main source or control in the northwest, alongside added local geological or environmental effects that shape the more intricate western pattern.

Fe: Iron (Fe) is mapped as a strongly focused feature, with a prominent high centered in the west-central portion of the area (Fig. 9). This hotspot is outlined by orange and red bands, where Fe rises above 0.05, representing the top observed values. Instead of an even spread, the map is clearly governed by this single zone of elevated accumulation.

One defining aspect of this distribution is the pronounced slope that rings the hotspot. In every direction—toward the east, the north, and the south—Fe values fall off quickly, shifting from greater than 0.05 to under 0.015 over a small distance. Such an abrupt drop underscores that the higher Fe amounts are narrowly restricted, with scant sign that they spread broadly across the study area.

Across most of the area—especially the eastern portion and the extreme northern and southern reaches—Fe remains very low, most often between 0 and 0.005. Still, narrow

tongues of somewhat higher readings (roughly 0.005 to 0.01) appear to run toward the north-northeast and to the southeast, implying only slight directional movement. Taken together, the arrangement points to one main western source, while showing little effect across the wider landscape.

As: Arsenic (As) appears in a strongly concentrated way, marked by a clear anomalous patch in the northwest part of the study region (Fig. 10). The main hotspot lies near 5.477 in longitude and 7.544 in latitude, where the highest values fall in the 0.038–0.046 range. Depicted with red and orange tones, this area corresponds to the greatest Arsenic levels shown on the map.

A striking characteristic here is the abrupt gradient around the hotspot. Moving away from the northwest, Arsenic drops off swiftly, passing through mid-level bands and then approaching nearly zero within a short span. This rapid falloff implies the higher values are closely bounded and do not carry far into the nearby surroundings.

Nearly the entire map area—most notably the east and south—shows essentially no Arsenic, with readings at or close to zero as conveyed by purple coloring. Aside from that, a small eastward reach of low values (about 0.002 to 0.004) appears near the central-west, indicating very limited spreading. In sum, the configuration is clearly uneven and favors a confined origin or geological influence in the northwest rather than a broadly distributed signal.

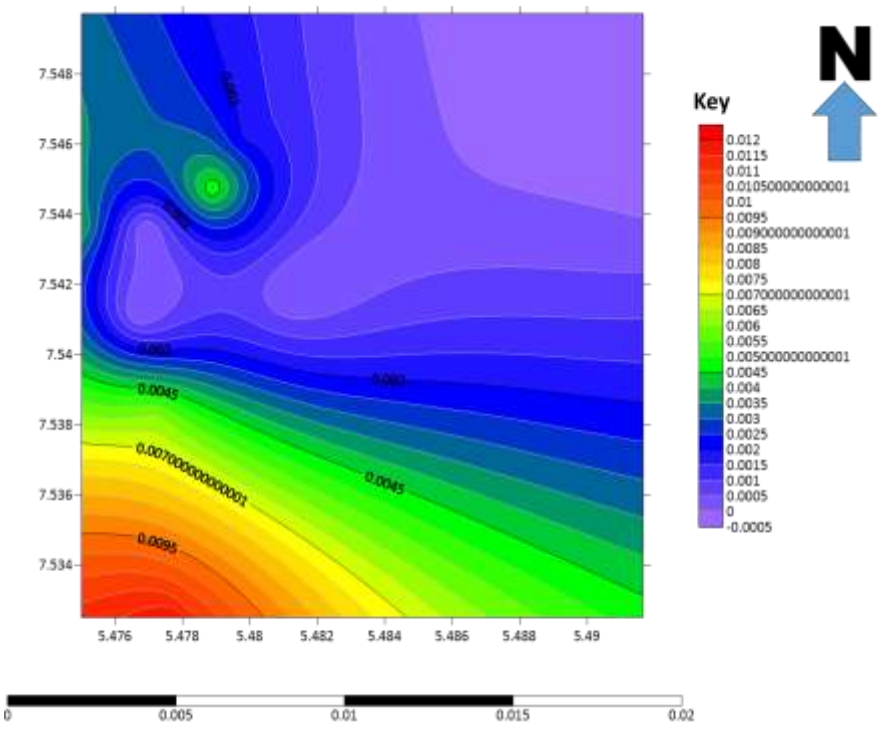

Figure 3: *Spatial distribution of Cu in the study area.*

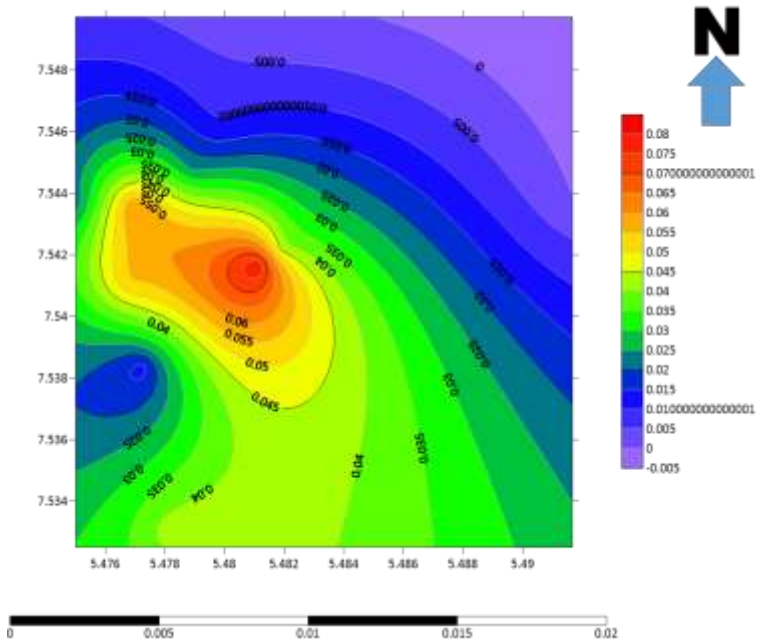

Figure 4: *Spatial distribution of Mn in the study area.*

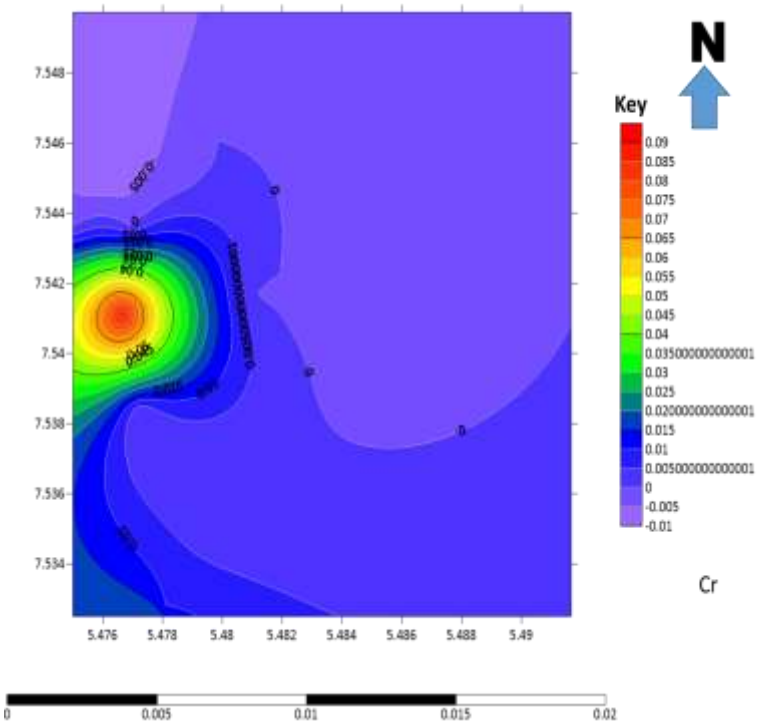

Figure 5: *Spatial distribution of Cr in the study area.*

International Journal of Earth & Environmental Sciences
Vol. 11, No. 1, 2026, pp. 134-157
http://ijees.ielas.org
ISSN: 2545-4161

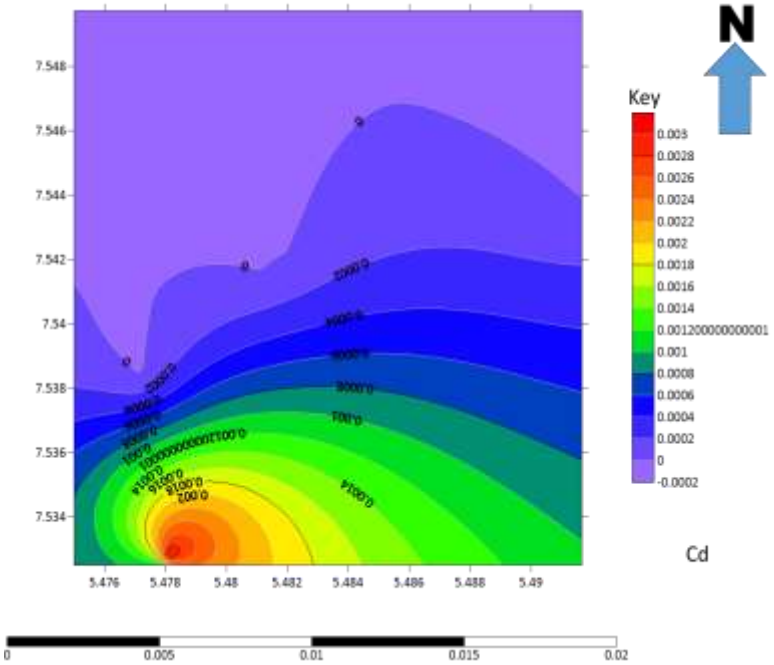

Figure 6: *Spatial distribution of Cd in the study area.*

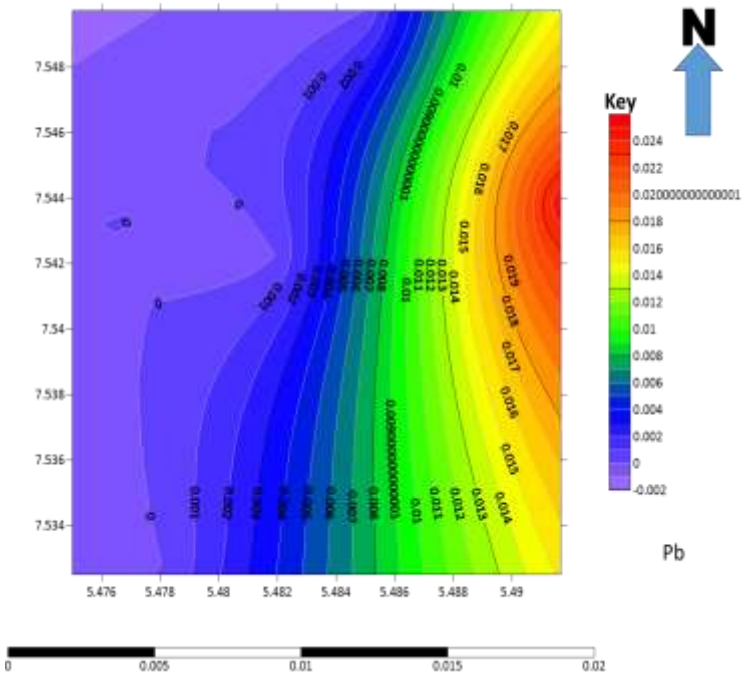

Figure 7: *Spatial distribution of Pb in the study area.*

International Journal of Earth & Environmental Sciences
Vol. 11, No. 1, 2026, pp. 134-157
http://ijees.ielas.org
ISSN: 2545-4161

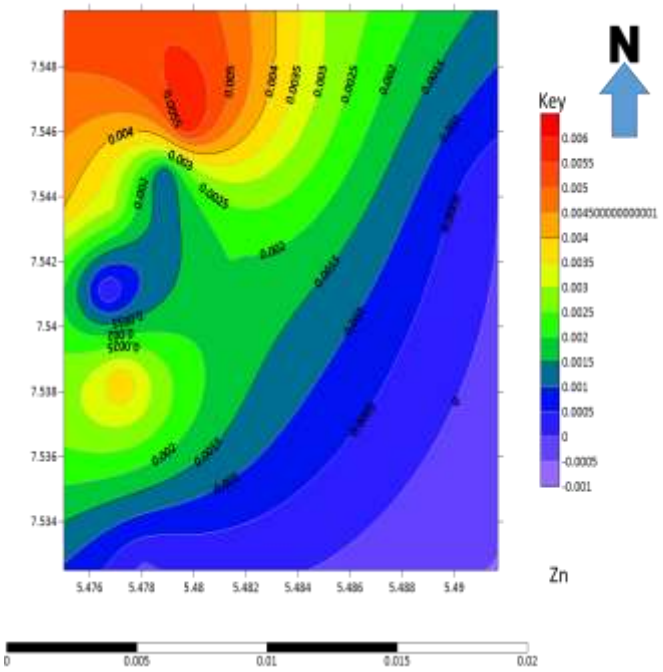

Figure 8: *Spatial distribution of Zn in the study area.*

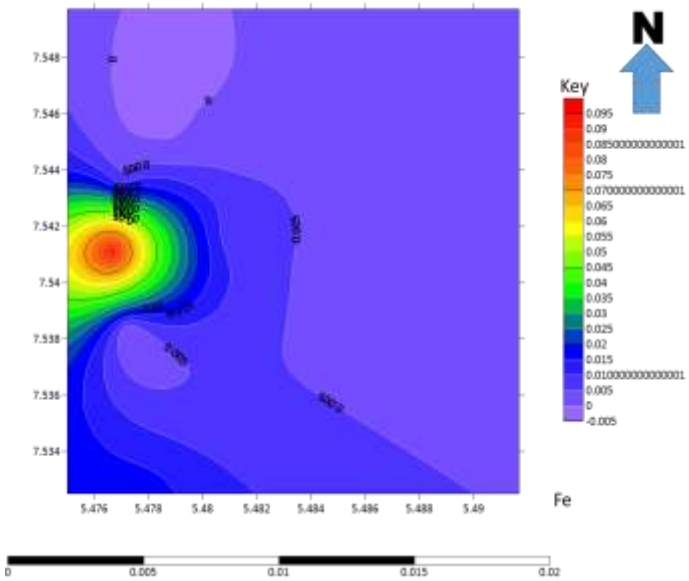

Figure 9: *Spatial distribution of Fe in the study area.*

International Journal of Earth & Environmental Sciences
Vol. 11, No. 1, 2026, pp. 134-157

http://ijees.ielas.org
ISSN: 2545-4161

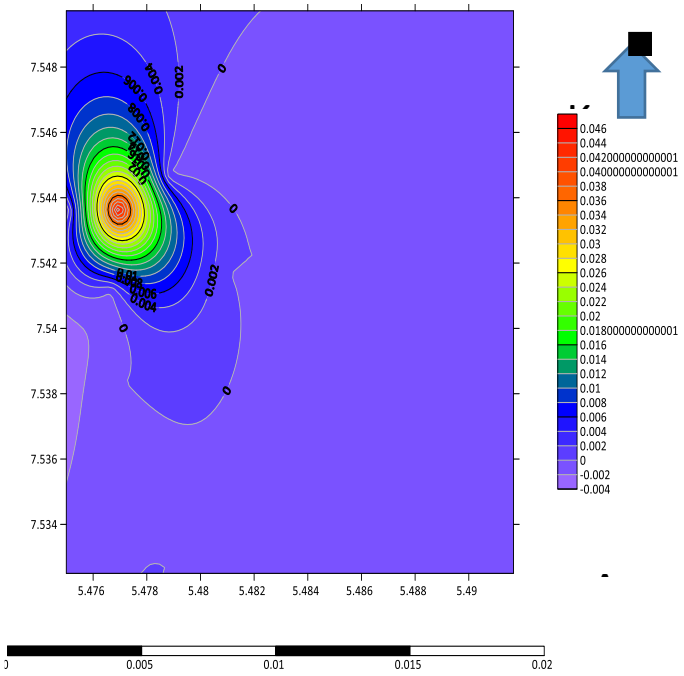

Figure 10: *Spatial distribution of As in the study area.*

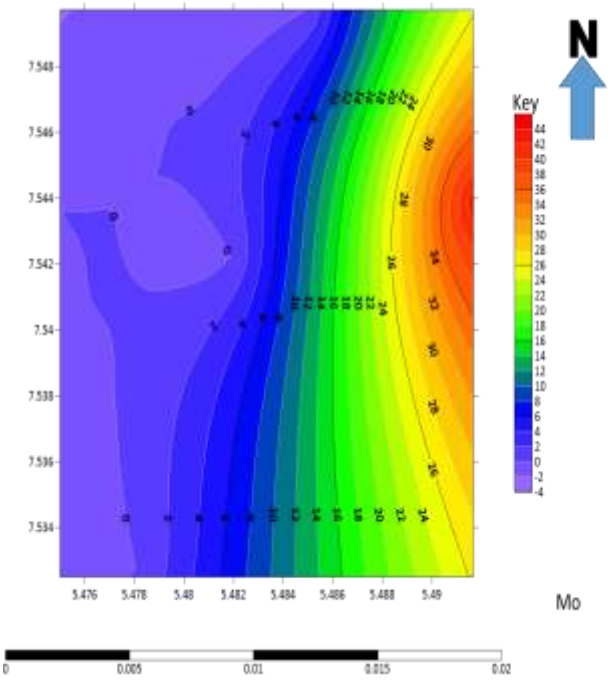

Figure 11: *Spatial distribution of Mo in the study area.*

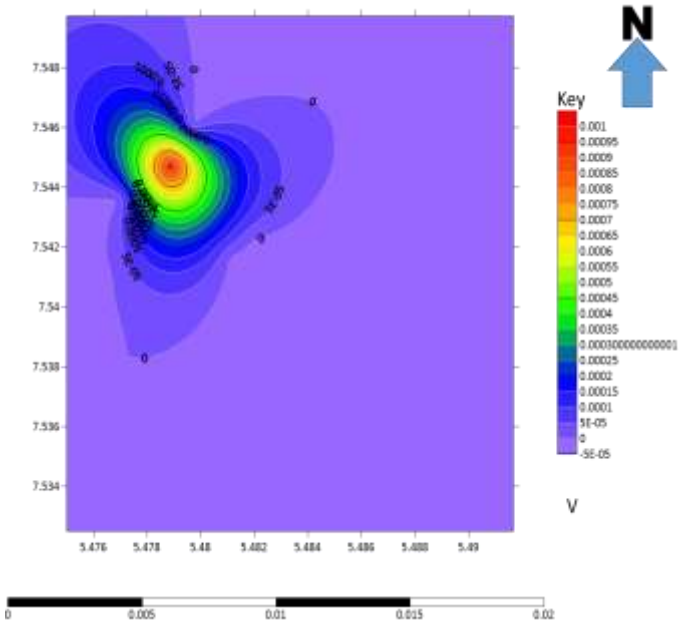

Figure 12: *Spatial distribution of V in the study area.*

Hydrogeochemical Significances

Table 5 presents a condensed hydrogeochemical assessment for the investigated region. Because heavy-metal levels are minimal, the points below are implied:

i. Natural Controls as the Main Driver

Metals present in the water mainly originate from breakdown of the surrounding rock materials. This further implies the site has no meaningful contamination linked to farming activities or industrial sources.

ii. Oxidation–Reduction Setting

Low measured values of iron and manganese may reflect only mildly oxidizing conditions, along with a small degree of dissolution under reducing environments.

iii. Aquifer characteristics

The groundwater-bearing unit probably consists of sediment-derived layers with little inherent metal loading. In addition, elevated bicarbonate levels, as indicated by earlier physicochemical findings, point to a lithology dominated by carbonates.

These parameters indicate a pristine groundwater system in the study area with dominance of natural geochemical processes.

Table 5
Comparison with Physicochemical Results

Parameter	Interpretation
Major ions:	Ca–HCO_3 type
Heavy metals:	Very low
Controlling process:	Rock weathering
Pollution level:	Minimal

Suitability for Potable Use

Considering the measured levels of heavy metals, the area's groundwater can be regarded as fit for human consumption with respect to trace-metal content. Every assessed chemical characteristic of the groundwater falls within the guideline thresholds published by the World Health Organization (2022). No urgent toxicological concern is evident.

Sodium Adsorption Ratio (SAR)

Across all collected groundwater samples, the calculated SAR values are consistently low, showing very limited sodium enrichment when set against calcium and magnesium amounts. This suggests that inputs from alkali metals contribute little to the total ionic makeup, and that alkaline earth constituents predominate within the groundwater system. SAR is commonly applied as a dependable indicator for assessing sodium-related risk in irrigation supplies (Food and Agriculture Organization (1985); United States Salinity Laboratory (1954)).

In agricultural terms, small SAR values point to irrigation water of good quality. Under these circumstances, the chance of sodium-driven soil dispersion is lowered, helping maintain soil integrity, permeability, and aeration. As a result, the groundwater is viewed as appropriate for irrigation, especially where soils are vulnerable to deterioration linked to sodicity (Food and Agriculture Organization, 1985).

In addition, the lack of high SAR readings shows that using this groundwater in farming does not present a meaningful sodium threat. This denotes minimal potential for gradual soil alkalization over time and aligns with continued irrigation use without harmful effects on soil physicochemical characteristics (United States Salinity Laboratory, 1954). The SAR diagram is shown in Figure 12.

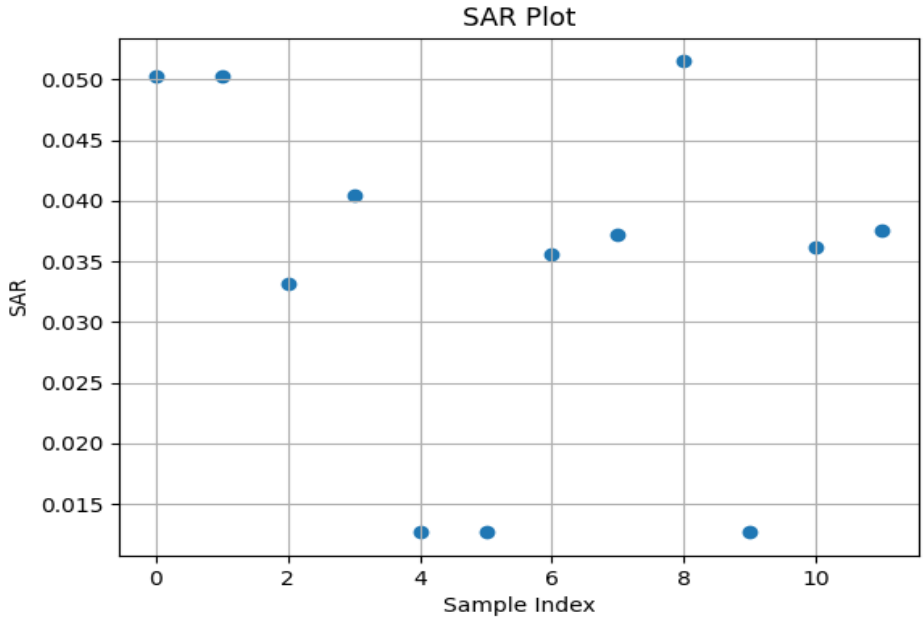

Figure 12: *SAR plot of the samples from the study area.*

Geochemical interpretation of groundwater using a Piper plot

Figure 13 presents the Piper chart depicting groundwater ionic composition. From how the plotted markers are arranged on the Piper graphic, the interpretations below can be drawn.

Cation Facies: In the cation triangle, the majority of samples group near the Ca2+ and Mg2+ side, implying a water category dominated by Ca–Mg.

Anion Facies: The samples are chiefly characterized by Cl− together with HCO3−, while SO42− levels remain very low at every sampling location.

Hydrochemical Facies: Within the central diamond, the plotted points fall in the upper-left sector, a position commonly associated with a mixed Ca–Mg–Cl class. This also points to groundwater in which alkaline earths are greater than alkalies, and strong acids are greater than weak acids.

This hydrochemical pattern indicates comparatively mineralized groundwater, probably shaped by nearby lithologic attributes of the Benin Formation.

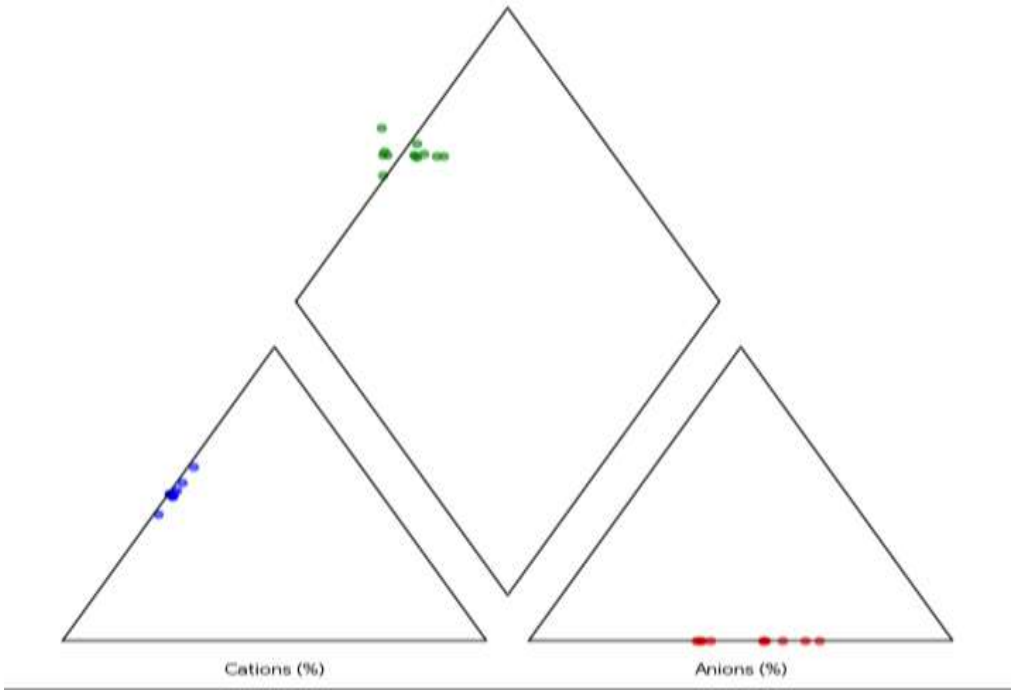

Figure 13: *Piper diagram for the hydrochemical analysis of the samples.*

Gibbs Diagram

Every groundwater sample evaluated falls within the rock-controlled zone on the Gibbs Diagram, as illustrated in Figure 14. From this, it follows that the geology exerts the main control over hydrochemical characteristics. The way the points are distributed implies that aquifer-material breakdown through dissolution and weathering is the key set of geochemical mechanisms driving ion buildup in the groundwater system.

The tight grouping also indicates that inputs from rainfall and from evaporation with subsequent crystallization play a comparatively small role. As a result, the chemical makeup of the groundwater is determined chiefly by interactions between water and surrounding rock, especially dissolution of minerals, which regulates the release and spatial distribution of the principal ions within the aquifer.

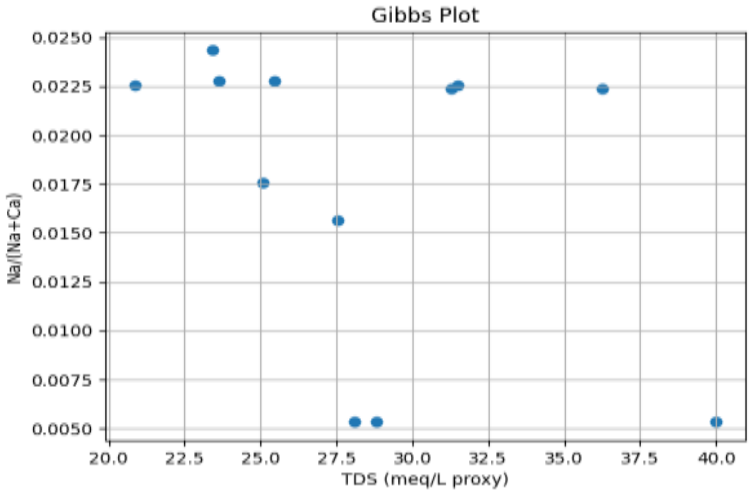

Figure 14: *Gibbs plot of the samples from the study area.*

Environmental and Health Implications

Groundwater chemistry in the investigated region does not exhibit clear evidence of pollution linked to factories or high-input farming. This conclusion is supported by the small amounts of ions that often signal contamination, including Chloride and Sulfate, along with the lack of unusual chemical buildup commonly tied to human sources.

The fact that the dissolved constituents are dominated by natural ions—especially calcium, magnesium, and bicarbonate—also implies that subsurface geology, not outside pollutants, mainly controls the water chemistry. Such a pattern fits a comparatively unspoiled hydrogeologic setting where reactions between water and surrounding rock are the key influence on groundwater makeup.

From the standpoint of human health, not finding measurable contamination implies the groundwater is, in general, appropriate for drinking. The observed chemistry does not point to harmful substances at concentrations that would create major health concerns. To confirm drinkability in accordance with World Health Organization criteria, a full evaluation is advised, incorporating microbiological testing and trace-element measurements.

For farming use, the groundwater appears similarly well suited. Because salinity is low and there is no indication of sodium-related risk, irrigation use would not damage soil structure or diminish crop yields. As a result, the supply can support ongoing agriculture without raising concerns about soil decline or lowered permeability.

In summary, the area's groundwater shows chemical stability and is mostly insulated from pollution caused by human activity. This highlights its dependability for both household needs and irrigation, while emphasizing that regular monitoring remains important for lasting sustainability and for spotting any developing contamination patterns early.

References

Adelana, S. M. A., and MacDonald, A. M. (2008). *Applied groundwater studies in Africa*. CRC Press.

Amos-Uhegbu, C., Igboekwe, M., Eke, K. and Eme, U. (2017). Evaluation of Groundwater Potential Using Integrated Geophysical Data in Parts of Michael Okpara University of Agriculture, Umudike, Southern Nigeria. *Advances in Research,* 10(3), 1-10; Article no.AIR.32121 ISSN: 2348-0394, NLM ID: 101666096 10. 1-10. 10.9734/AIR/2017/3.

Appelo, C. A. J., and Postma, D. (2005). *Geochemistry, groundwater and pollution* (2nd ed.). Balkema.

Egbueri, J. C. (2020). Evaluation of groundwater quality and human health risk in Nigeria. *Environmental Monitoring and Assessment*, 192, 1–20.

Egbueri, J. C., and Unigwe, C. O. (2020). Understanding groundwater contamination in Nigeria using multivariate statistics. *Groundwater for Sustainable Development*, 10, 100323.

Hem, J. D. (1985). Study and interpretation of the chemical characteristics of natural water. USGS.

Li, P., Wu, J., and Qian, H. (2019). Hydrogeochemical evolution and groundwater quality assessment. *Environmental Pollution*, 249, 618–629.

Obi, J. and Udoh, B. (2011). Identification of Soil Management Factors from Spatially Variable Soil Properties of Coastal Plain Sands in Southeastern Nigeria. *Open Journal of Soil Science*, **1**, 25-39. doi: 10.4236/ojss.2011.12004.

Subramani, T., Rajmohan, N. and Elango, L. (2010). Groundwater geochemistry and identification of hydrogeochemical processes. *Environmental Monitoring and Assessment*, 162, 123–137.

Ukah, B. U., Egbueri, J. C., & Unigwe, C. O. (2019). Hydrogeochemical evaluation of groundwater in southeastern Nigeria. *Applied Water Science*, 9, 1–16.

Pallavi, N., Atulya, K., M., Priyajit, S., Somnath K., and Patitapaban, M. (2023). Groundwater Quality, Hydrogeochemical Characteristics, and Potential Health Risk Assessment in the Bhubaneswar City of Eastern India. Water, Air, & Soil Pollution, 9. DOI 10.1007/s11270-023-06614-z.

Zhang, Q., Xu, P., Qian, H., et al. (2018). Assessment of groundwater quality and human health risk. *Human and Ecological Risk Assessment*, 24(7), 1854–1871.

UNESCO (2022). *United Nations World Water Development Report 2022: Groundwater: Making the invisible visible*.

United Nations Educational, Scientific and Cultural Organization (2019). *World Water Development Report*.

WHO (2017). *Guidelines for drinking-water quality* (4th ed.).